International Reviews in Physical Chemistry
Vol. 27, No. 1, January–March 2008, 27–51

Taylor & Francis
Taylor & Francis Group

REVIEW ARTICLE

Photoelectron spectra of hydrated electron clusters *vs.* cluster size: connecting to bulk

James V. Coe[a]*, Shaun M. Williams[a] and Kit H. Bowen[b]

[a]*Department of Chemistry, The Ohio State University, Columbus, OH 43210-1173, USA;*
[b]*Department of Chemistry, The Johns Hopkins University, Baltimore, MD 21218, USA*

(*Received 10 August 2007; final version received 30 October 2007*)

Connecting cluster properties to bulk can result in new insights, both for the bulk and for clusters, and this is especially the case for the hydrated electron, e^-(aq), and its cluster counterparts. In bulk, e^-(aq) can be viewed as an anionic defect state of pure water, which is itself a large-band-gap semiconductor. Thus, when properly extrapolated to bulk, the properties of $(H_2O)_n^-$ clusters must reflect important energetic properties of bulk water. Several of these have been extracted and are presented here. As for the nature of $(H_2O)_n^-$ clusters themselves, the topic has now inspired spirited debate for over two decades. Here, we offer our perspective on these intriguing entities. Among several isomeric groups of $(H_2O)_n^-$ and $(D_2O)_n^-$ clusters, the one having the highest electron binding energies (herein called bulk embryonts) has been extrapolated to deduce the implied photoelectron spectrum of the bulk hydrated electron. The legitimacy of the lineshape fitting procedures used here is supported by the successful extrapolation of cluster absorption data to its known bulk benchmarks.

Keywords: Connecting to bulk; Hydrated electron clusters; Photoelectron spectroscopy

Contents

*Corresponding author. Email: coe.1@osu.edu; kbowen@jhu.edu

ISSN 0144–235X print/ISSN 1366–591X online

DOI: 10.1080/01442350701783543
http://www.informaworld.com

1. Introduction

Since extrapolations of cluster properties must ultimately be consistent with their corresponding bulk properties, $(H_2O)_n^-$ clusters will eventually grow into bulk hydrated electrons as $n \to \infty$. Thus, the study of $(H_2O)_n^-$ clusters as a function of size, n, provides step-by-step insight into the evolution of electron hydration in the finite size regime. Three isomeric forms of $(H_2O)_n^-$ clusters have been observed experimentally and classified into groups according to their relative electron binding energies. In the two groups with the lowest electron binding energies, their excess electrons are likely to be associated, in one way or another, with their cluster surfaces. Since the bulk hydrated electron (a defect state of macroscopic water) is by definition an internalized electron state, the properties of these two groups are not expected to extrapolate to the properties of the bulk hydrated electron. On the other hand, the nature of the third group, i.e. the one exhibiting the highest electron binding energies and the one herein referred to as 'bulk embryonts', is much less certain and has, in fact, stirred spirited debate for over two decades. The persistent question concerns whether the excess electrons in this third, high binding energy group are sufficiently internalized to begin to mimic some of the essential properties of the hydrated electron. The evidence has gone back and forth on this issue. The $n^{-1/3}$ dependence of vertical detachment energy values from our photoelectron work (Coe 1986;[1] Arnold, Coe *et al.* 1990;[2] Coe and Lee *et al.* 1990;[3] Lee and Arnold *et al.* 1991;[4] Haberland and Bowen 1994;[5] Castleman and Bowen, 1996;[6] Coe and Earhart *et al.* 1997;[7] Coe and Arnold *et al.* 2006)[8] suggested a significant degree of internalization beyond $n = 11$ or so. Theoretical work disagreed.[9–11] Then, relatively recently, new photoelectron[12] and time-domain[13] work both tended to support the internalization hypothesis, but this was again soon challenged by new theoretical work.[14]

Using extrapolated photoelectron results to further elucidate the internalization issue is complicated by the lack of corresponding bulk properties for the hydrated electron, e.g. while the absorption spectrum of the bulk hydrated electron is known, its photoelectron

spectrum is not. Nevertheless, a wealth of information can be extracted from the photoelectron lineshapes of $(H_2O)_n^-$ spectra,[8] much more than just their peak centres which were the focus of our earlier work.[3] Here, we have extrapolated lineshape parameters to bulk to yield the implied photoelectron spectrum of the bulk hydrated electron. These parameters are the peak intensity (A), the peak energy position (E_{max}), the Gaussian peak width to the low-energy side (σ_G), and the Lorentzian peak width to the high-energy side (σ_L), which together are known[15,16] to provide a good fit to the bulk absorption spectrum of e^-(aq). In addition to having important implications about internalization, the analysis presented herein relates $(H_2O)_n^-$ cluster absorption and photoelectron data and leads to reassessments of important bulk water properties, such as its liquid electron affinity and the location of excess electron p-states relative to the conduction band.

Extrapolation to bulk hydrated electron properties is also complicated by the unusual, but well-characterized, temperature dependence of the bulk absorption spectrum. The spectrum shifts dramatically to the blue with cooling, and yet maintains its lineshape over a very wide range of temperatures and pressures. The bulk absorption spectrum is a 'moving target' unless a temperature is specified. Temperature is also very important with regard to the clusters. Several groups[12,17] now have photoelectron results which show how the temperature of the ion source can favour the production of less-internalized clusters over more-internalized clusters. We need to determine a characteristic temperature for the clusters in order to connect to bulk. This task is more reliably accomplished if one uses several properties in addition to peak centres, i.e. average kinetic energy and radius of gyration of the excess electron, both extractable from the full lineshape with moment analysis.

The words 'photoelectron' and 'photoemission' have different meanings to different readers. In this work, 'photoelectron' refers to the use of a fixed photon energy with measurement of the intensity of photodetached electrons as a function of their electron binding energy. 'Photoemission' will refer to the intensity of photodetached electrons as the photon energy is scanned. Conventional absorption spectroscopy involves scanning the photon energy and measuring the disappearance of photons without regard to the bound or free nature of the product electrons. Consequently, photon-scanned absorption and photon-fixed photoelectron spectra appear very different in general. In this work, we observe that the cluster absorption and photoelectron spectra are quite similar in lineshape, and that they can be fit with the same lineshape function. This surprising observation holds over the whole range of cluster size, but it is not a coincidence as it results from the Franck–Condon factors of solvent orientation as projected onto the upper electronic states (conduction band and p-states).

The paper is organized as follows: we begin with a description of the lineshape fitting parameters, followed by a summary of past work on the temperature dependence of the bulk hydrated electron's absorption lineshape parameters. Then, there is a brief description of lineshape moment analysis and a characterization of the temperature dependence of the average kinetic energy and radius of gyration of the bulk hydrated electron. Armed with a temperature-dependent set of bulk absorption peak centres, average kinetic energies, and radii of gyration, we simultaneously fit the three corresponding cluster properties (extracted from the cluster absorption lineshapes with moment analysis) using the constraint that the bulk intercepts must correspond to the same temperature. This process assigns a temperature (in an average sense) to both the

cluster data and results extrapolated from the cluster data, as well as providing information about the size of the excess electron as the clusters grow. Finally, we take the cluster photoelectron lineshape parameters and extrapolate them to bulk to obtain the central result, the implied bulk photoelectron spectrum of the hydrated electron which may also be taken as the bulk photoemission spectrum.

2. Describing the lineshape parameters

The $(H_2O)_n^-$ cluster photoelectron and absorption spectra were fit[8] to the same functional form that is well-known to fit the bulk e^-(aq) absorption spectrum. Many more elaborate forms have been employed for hydrated electron absorption spectra,[15,18] but we required a simple form to untangle multiple isomers that didn't assume bound to free transitions (as there is now overwhelming evidence for bound p-states).[13,19–27] The ultimate justification for this empirical form is that it works very well. The fitting function, $I(E)$, has a Gaussian form to the low-energy side of the prominent (origin) peak and a Lorentzian form to the high-energy side:[15,16]

$$\begin{cases} I(E) = Ae^{-1/2((E-E_{\max})/\sigma_G)^2} & \text{if } E \le E_{\max} \\ I(E) = A\dfrac{1}{1+[(E-E_{\max})/\sigma_L]^2} & \text{if } E \ge E_{\max} \end{cases} \quad (1)$$

where $E_{\max}$ is the energy position of the intensity maximum, E is electron binding energy for photoelectron spectra and photon energy for absorption spectra, σ_G is the Gaussian standard deviation characterizing the origin's width on the low-energy side of the peak (full-width-at-half-maximum divided by 2.354 in a full Gaussian lineshape), σ_L is the origin's Lorentzian width parameter characterizing the high-energy side (half-width-at-half-maximum for a full Lorentzian lineshape), and A is the intensity maximum.

3. Characterizing the bulk hydrated electron

3.1. *Bulk absorption lineshape of the hydrated electron* vs. *temperature*

The peak maximum ($E_{\max}$) of the bulk hydrated electron absorption spectrum shifts to the blue with cooling, while the lineshape is fairly insensitive to temperature. We have taken lineshape parameters of the bulk absorption spectra *vs.* temperature from two sources. The first is an extensive study by Tuttle and Golden[16] in which spectra were collected under a variety of temperatures and pressures from a number of investigators. We fit the peak centres to temperature (T) (at 1 atm as tabulated in this work) giving Equation (2a). Tuttle and Golden overlayed and shifted the spectra to align the peak centres revealing a remarkably similar lineshape over a large range of temperature and pressure, i.e. shape stability. We digitized the overlay in their[13] Figure 4 and fit it to Equation (1) giving Equations (3a) and (4a). Shape stability[16,28–31] corresponds to σ_G and σ_L being constant with respect to temperature. These three equations allow one to generate the bulk absorption spectrum valid for any conditions within the range of observations (269–380 K, 0.001–6.26 kbar):

$$E_{\max,\,\mathrm{ABS,\,bulk,\,H2O}} = 2.585(34) - 0.00290(11)T \quad (2a)$$

$$\sigma_{G,\,ABS,\,bulk,\,H_2O} = 0.3041(15)\text{eV} \tag{3a}$$

$$\sigma_{L,\,ABS,\,bulk,\,H2O} = 0.4951(25)\text{eV} \tag{4a}$$

where E_{max} has units of eV and T has units of K. The uncertainties are given in parentheses as the least significant figures (here and throughout). The cluster anions under study in this work are colder than the above temperature range warranting a still closer examination of the bulk lineshapes. Thus, we also summarize a study by Jou and Freeman[15,77] on the spectral widths using data at 1 atm and from 274–380 K giving:

$$E_{max,\,ABS,\,bulk,\,H_2O} = 2.4506 - 0.0024T \tag{2b}$$

$$\sigma_{G,\,ABS,\,bulk,\,H_2O} = 0.1517 + 0.00051T \text{ or } 0.161(10)T^{1/2} \tag{3b}$$

$$\sigma_{L,\,ABS,\,bulk,\,H_2O} = 0.5124 - 0.0001T \tag{4b}$$

where E_{max}, σ_G, and σ_L are in eV and T is in K. We use the letters 'a' and 'b' in the equation numbers to distinguish similar properties determined with Tuttle–Golden and Jou–Freeman data sets, respectively. Jou and Freeman essentially found no temperature dependence for σ_L, but a small temperature dependence for σ_G. The $T^{1/2}$ option in Equation (3b) might be more physical for extrapolation beyond the experimental temperature range. There is little difference in the predicted spectra from either data set within the range of experimental conditions in which bulk absorption spectra were recorded, but the differences are more pronounced at lower temperatures.

The spectrum of the bulk hydrated electron in fully deuterated water can also be characterized in a similar fashion. The 'shape stability' parameters extracted by digitizing Figure 6 in Tuttle and Golden[16] are given in Equations (6a) and (7a). Deuterated peak centres (E_{max}) were fit *vs.* temperature using the Jou and Freeman data giving Equation (5a). The absorption spectra of the bulk hydrated electron in D_2O can be generated with the following set of equations:

$$E_{max,\,ABS,\,bulk,\,D_2O} = 2.482(50) - 0.00244(12)T \tag{5a}$$

$$\sigma_{G,\,ABS,\,bulk,\,D_2O} = 0.3010(8)\text{eV} \tag{6a}$$

$$\sigma_{L,\,ABS,\,bulk,\,D_2O} = 0.4488(14)\text{eV}. \tag{7a}$$

While the Gaussian width (σ_G) is the same with or without deuteration, the deuterated Lorentzian width (σ_L) reduces to 90.6% of the non-deuterated value, suggesting a role for nuclear motion in this part of the lineshape. Basically the deuterated maximum occurs ~30 meV higher in binding energy at any specific temperature than the non-deuterated maximum.[15]

3.2. *Brief description of moment analysis*

The temperature of the water cluster anions needs to be characterized on average in order to gauge the progress of cluster convergence towards bulk. In fact, a more

complete characterization can be obtained if one studies the whole cluster lineshape, rather than just peak centres. To this end, we have considered moment analysis[29,32–34] of the spectral lineshapes. There are sum rules that relate the spectral moments to properties of the ground state, such as average kinetic energy and radius of gyration of the excess electron. Spectral moments (indexed by k) are defined as[32]

$$S(k) = n_0 \int_0^\infty \omega^k \gamma(\omega) \mathrm{d}\omega \tag{8}$$

where n_0 is the solvent refractive index, ω is the spectral angular frequency, and $\gamma(\omega)$ is the spectral density of oscillator strength, i.e. a normalized absorption lineshape which we can get experimentally from fits to the Gaussian/Lorentzian lineshape defined by $I(E)$ in Equation (1) and lineshape parameters developed in Section 3.1. The empirical form of I(E) is not rigorously valid in the extreme wings of the spectrum[32,34] so in practice the lineshapes were numerically integrated from 0.1 to 8 eV. As a result, moments with $k > 1$ are not as reliably determined. Normalization constants, N, were found with the Equation (1) spectral profiles given as a function of energy in eV, such that the integration for the $k = 0$ moment produced a value of 1:[32]

$$S(0) = n_0 \int_0^\infty \frac{I(E)}{N} \mathrm{d}E = 1 \text{ or } N/n_0 = \int_0^\infty I(E) \mathrm{d}E. \tag{9}$$

The mean squared dispersion $\langle r^2 \rangle$ of the excess electron in its ground state is related to the $k = -1$ moment as[32]

$$S(-1) = \int_0^\infty \frac{27.21}{E} \frac{I(E)}{N/n_0} \mathrm{d}E = \frac{2}{3} \langle r^2 \rangle \tag{10}$$

where E is in eV, and $\langle r^2 \rangle$ in Bohr^2. With an s-like ground state, the dispersion is often reported as $\sqrt{\langle r^2 \rangle}$, the radius of gyration, which is useful as it can also be determined with theoretical models. The average kinetic energy, $\langle KE \rangle$, of the hydrated electron's ground state can be obtained from the $k = +1$ moment as[32]

$$S(+1) = \int_0^\infty E \frac{I(E)}{N/n_0} dE = \frac{4}{3} \langle KE \rangle \tag{11}$$

where both E and $\langle KE \rangle$ are in eV.

3.3. *Moment analysis of the bulk hydrated electron absorption spectrum*

Analytical functions for the experimental bulk hydrated electron absorption lineshapes can be generated at any temperature with Equations (2)–(4) from the previous section. We performed moment analysis with such lineshapes at a set of temperatures to obtain the radius of gyration [Equation (10)] and average kinetic energy [Equation (11)] at a set of temperatures. The results were summarized by fitting to polynomials in temperature giving:

$$\sqrt{\langle r^2 \rangle_{bulk,\,Tuttle}} = 1.999(5) + 8.6(5)x10^{-4}T + 1.94(13)x10^{-6}T^2 \tag{12a}$$

$$\sqrt{\langle r^2\rangle_{bulk,\,Freeman}} = 1.947(10) + 1.21(12)x10^{-3}T + 1.59(28)x10^{-6}T^2 \quad (12b)$$

$$\langle KE\rangle_{bulk,\,Tuttle} = 2.2730(4) - 0.002103(2)T \quad (13a)$$

$$\langle KE\rangle_{bulk,\,Freeman} = 2.344(13) - 0.00301(15)T + 1.46(37)x10^{-6}T^2 \quad (13b)$$

where $\sqrt{\langle r^2\rangle}$ is in Å, $\langle KE\rangle$ in eV, and T in K. Both lineshapes from Tuttle–Golden[13] data [Equations (2a), (3a), (4a)] and Jou–Freeman[12] data [Equations (2b), (3b), (4b)] were used for input as a check of consistency. The radius of gyration and average kinetic energy can be combined with the peak centre information to allow a more comprehensive evaluation than is available with peak centres alone.

4. Connecting the cluster data to bulk

The lineshape fit parameters for the photoelectron spectra of $(H_2O)_n^-$ and $(D_2O)_n^-$ bulk embryont species come from our previous paper[8] (Table 3). Fits of this sort have been accomplished for the absorption spectra of $(H_2O)_n^-$ by Johnson and coworkers,[30,32] see Figures 1 and 2 of ref. 35 but we are unaware of a published tabulation of the fit parameters. Those presented in Table 1 were obtained by digitizing and fitting the action spectra of Ayotte and Johnson.[35]

4.1. $(H_2O)_n^-$ *cluster absorption lineshape* vs. *size*

We now proceed to characterize the same set of lineshape parameters and properties extractable from lineshapes for the $(H_2O)_n^-$ cluster absorption spectra that we earlier obtained for the bulk hydrated electron. Absorption lineshapes generated from the parameters in Table 1 were analysed with moment analysis for the radius of gyration and average kinetic energy, and the results are presented in the far right columns of Table 1. All three quantities (E_{max}, $\sqrt{\langle r^2\rangle}$, and $\langle KE\rangle$) progress smoothly to bulk as expected for the bulk embryont group, but with some noise due to the difficulty of the experiment. The specific bulk value, to which these three properties connect, is a strong function of temperature. If one fits any of these quantities alone *vs.* $n^{-1/3}$, there is a significant amount of uncertainty in the bulk intercept and the intercept of one quantity may not pertain to the same temperature as the others. To address this issue, we simultaneously fit all three properties, constraining the intercepts to pertain to the same temperature [as set by the fits of Equations (2a), (12a), and (13a)]. This approach builds on issues examined by Bartels regarding moment analysis[34] by adding temperature consistency to the process of connecting to bulk and reducing the effect of noise in any particular property. In the global fit, all values of E_{max} were weighted by an uncertainty of 0.021 eV, and the weights for the $\sqrt{\langle r^2\rangle}$ and $\langle KE\rangle$ data came from Monte Carlo propagation of errors in E_{max}, σ_G, and σ_L. The best fit is obtained for a temperature of 210 K, which we take as an average characterization over cluster size. The resultant fit expressions of $\sqrt{\langle r^2\rangle}$, $\langle KE\rangle$, and E_{max} *vs.* cluster size (n) for the cluster absorption data (at 210 K) are given in Equations (14)–(16). The radius of gyration is in Å with an estimated standard deviation (esd) of 0.07 Å, $\langle KE\rangle$ is in eV with an esd of 0.07 eV, and $E_{max,ABS}$ is in eV with an esd of 0.04 eV. Bulk values at

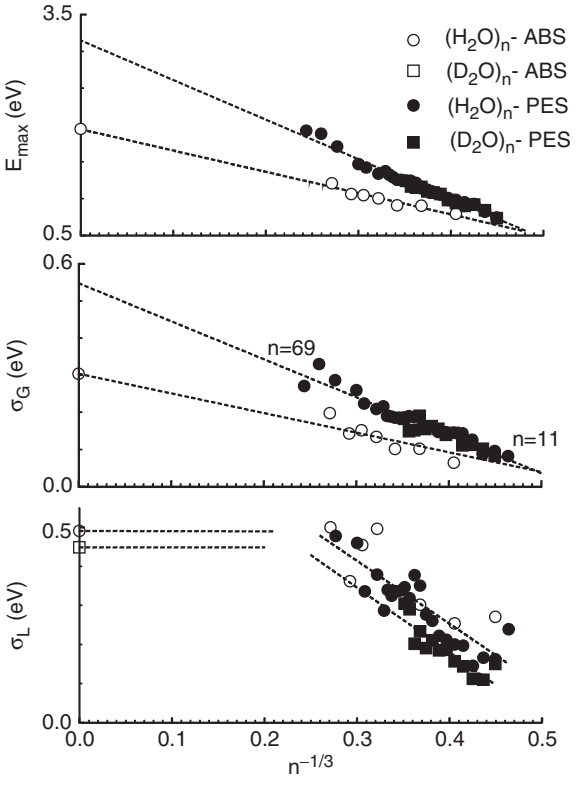

Figure 1. Bulk embryont lineshape parameters, $E_{\max}$, σ_G, and σ_L, [from equation (1)] *vs.* $n^{-1/3}$ where n is the number of waters. The top plot is of peak centres ($E_{\max}$), the middle is of the Gaussian widths (σ_G) of the low-energy side, and the bottom is of Lorentzian widths (σ_L) of the high-energy side. Parameters of the $(H_2O)_n^-$ absorption spectra are shown with open circles, those of $(H_2O)_n^-$ photoelectron spectra are shown with closed circles, and those of $(D_2O)_n^-$ photoelectron spectra are shown with closed squares. The absorption spectra parameters have known bulk properties providing clues to how the cluster properties progress towards bulk.

$T = 210\,\mathrm{K}$ are given in Table 1 for both the Tuttle/Golden[16] and Jou/Freeman[15] temperature constraints, so that the reader can gauge the size of systematic effects due to these different perspectives. The differences are not very important at 210 K, but would be more important at lower temperatures.

The $E_{\max}$, σ_G, and σ_L absorption lineshape parameters are presented in Figure 1 with open symbols. Once we know the temperature, we can fix the bulk value of the Gaussian widths, σ_G, at 0.304 (extrapolating to 210 K from Tuttle and Golden) or 0.259 (extrapolating to 210 K from Jou and Freeman data). Equation (17) gives the σ_G fit *vs.* $n^{-1/3}$, where σ_G is in eV with an esd of 0.021 eV. Unlike the $E_{\max}$ and σ_G parameters (top and middle of Figure 1), the Lorentzian widths (σ_L) of both the absorption and photoelectron $(H_2O)_n^-$ cluster data sets are extensively overlapped (see bottom of Figure 1). The fit of σ_L (in eV) *vs.* $n^{-1/3}$ of the absorption $(H_2O)_n^-$ set gives –1.4(4) $n^{-1/3} + 0.84(14)$ with an esd of 0.06 eV. It reaches the bulk value at $n \approx 67$. The same fit of

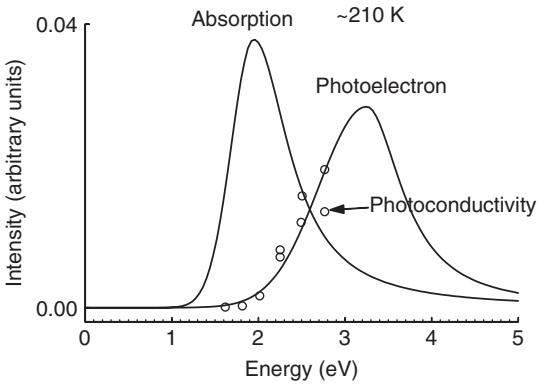

Figure 2. The absorption spectrum of the bulk hydrated electron at 210 K plotted with the photoelectron spectrum of the bulk hydrated electron obtained by extrapolating the cluster properties. Kevan's photoconductivity data (open circles) are also shown for comparison to the photoelectron threshold region. Kevan's data was recorded at 77 K, so it has been corrected to 210 K by shifting it by –0.32 eV according to equation (2a). Both photoconductivity and photoelectron threshold regions fall on top of each other providing the most compelling evidence to date that V_0 is about 0.0 eV in ice.

Table 1. Lineshape fit parameters as given in equation (1) for $(H_2O)_n^-$ absorption spectra from Ref. 35 and the results of moment analysis on the fitted lineshapes. Estimated standard deviations of the lineshape parameters from the fitting procedure alone are given in parenthesis as the least significant figures. These errors underestimate the actual errors as judged by global fits of the parameters, but they provide a good sense of relative variations through the data set. Globally, we find the estimated standard deviations of E_{max}, σ_G, σ_L to be 0.037, 0.020, and 0.050 eV, respectively. The estimated standard deviations in the radius of gyration and average kinetic energy come from a Monte Carlo analysis based on the error distributions of the lineshape parameters as input.

n # of waters in $(H_2O)_n^-$	σ_G Gaussian peak width (eV)	σ_L Lorentzian peak width (eV)	E_{max} Peak centre (eV)	A peak intensity (e^- counts)	$\sqrt{\langle r^2 \rangle}$ Radius of gyration (Ang.)	$\langle KE \rangle$ Kinetic energy (eV)
11	NA	0.271	NA	~15		
15	0.0647(21)	0.254(5)	0.7950(18)	19.9(2)	3.321(19)	0.902(10)
20	0.1022(24)	0.302(7)	0.9046(24)	12.1(1)	3.159(22)	0.998(14)
25	0.1016(18)	0.336(6)	0.9096(19)	14.8(1)	3.114(16)	1.037(10)
30	0.1341(28)	0.496(16)	1.005(3)	10.8(1)	2.897(27)	1.215(23)
35	0.152(4)	0.455(19)	1.048(4)	12.2(2)	2.905(31)	1.199(25)
40	0.143(3)	0.362(14)	1.063(4)	13.0(2)	2.946(29)	1.133(22)
50	0.198(5)	0.50(5)	1.21(6)	12.2(2)	2.751(60)	1.321(58)
∞@210K[a]	0.304	0.495	1.977		2.279	1.775
∞@210K[b]	0.259	0.491	1.947		2.268	1.785

Notes: [a]From Tuttle and Golden.[16]
[b]From Jou and Freeman.[77]

the photoelectron $(H_2O)_n^-$ set gives –2.0(3) $n^{-1/3} + 1.02(11)$ with an esd of 0.06 eV. It reaches the bulk absorption value at $n \approx 55$ (the bulk photoelectron σ_L value is unknown). Given the scatter in the σ_L results and the low signal of the raw cluster absorption spectra, there is low confidence in the differences of these two fits. Both sets

were also combined and fit to $n^{-1/3}$ giving Equation (18) where σ_L is in eV with an esd of 0.05 eV. This gave a slight improvement over the individual fits and is the fit pictured in Figure 1 (lowest panel). The photoelectron and absorption spectra of $(H_2O)_n^-$ share a similar Lorentzian width (and trend with width) at any given cluster size to within the scatter of the data sets. The following set of equations characterizes the lineshapes and lineshape extractable parameters of the $(H_2O)_n^-$ cluster absorption spectra at a temperature of 210 K:

$$\sqrt{\langle r^2 \rangle_{ground\ state}}(n) = 2.265 + 1.203n^{-1/3} + 3.396n^{-2/3} \tag{14}$$

$$\langle KE \rangle_{ground\ state}(n) = 1.832 - 2.272n^{-1/3} \tag{15}$$

$$E_{\max}, \mathrm{ABS}(n) = 1.977 - 2.986n^{-1/3} \tag{16}$$

$$\sigma_{\mathrm{G,\ ABS}}(n) = -0.528(5)n^{-1/3} + 0.304 \tag{17}$$

$$\sigma_{\mathrm{L,\ ABS/PES,\ H_2O}}(n) = -1.61(18)n^{-1/3} + 0.90(7) \text{ for } n \leq\sim 60. \tag{18}$$

4.2. $(H_2O)_n^-$ *and* $(D_2O)_n^-$ *cluster photoelectron lineshape* vs. *size*

We now turn to the characterization of the cluster photoelectron lineshapes *vs.* cluster size for the bulk embryonts. The lineshape parameters, $E_{\max}$, σ_G, and σ_L, are presented for both the absorption and photoelectron data sets in Figure 1, where open circles represent the $(H_2O)_n^-$ absorption data,[35] closed circles represent the $(H_2O)_n^-$ photoelectron data, and closed squares represent the $(D_2O)_n^-$ photoelectron data. Bulk parameters are available for the absorption data and can be seen plotted at $n^{-1/3} = 0$.

Peak centres: The photoelectron peak centres (VDEs) were fit *vs.* $n^{-1/3}$ for the non-deuterated data alone without fixing the slope or intercept, this giving Equation (19) where $E_{\max}$ is in eV with an estimated standard deviation of 0.035 eV. The dielectric $n^{-1/3}$ slope is expected to range from[37] –5.6 to –5.9 eV based on the variation of the static and optical dielectric constants of water/ice with temperature. The experimental slope of –5.65 eV falls within this range. A value of –5.73 eV was originally reported[3] using fits to asymmetric Gaussians. Since the deuterated photoelectron peak centres are virtually indistinguishable from the non-deuterated (see the top of Figure 1), both were also fit together giving equation (20) where, again, $E_{\max}$ is in eV. This procedure produces a slightly diminished slope because of the lower average cluster size of the deuterated data (evidence for gradual internalization, see section 6.5). The fit lines of the absorption and photoelectron peak centres intersect at $n = 11$ and smoothly diverge with increasing cluster size to their separate bulk intercepts. Since abrupt transitions in excess electron internalization with size would be evident in both the absorption and photoelectron spectra, the smooth progression in the absorption peak centres to a known bulk value reveals no such transitions and assures that the photoelectron peak centres also progress smoothly to bulk. The smooth progression of the photoelectron data with the continuum law limiting slope gives confidence that the VDEs are progressing smoothly (without transitions) to a

meaningful bulk intercept, $VDE_\infty = 3.25 \pm 0.06$ eV. In section 6.5, we re-evaluate this intercept by allowing for gradual internalization of the excess electron using the radius of gyration of equation (14) as an indicator of the size of the excess electron.

The Gaussian widths: The non-deuterated photoelectron Gaussian widths, σ_G, were indistinguishable from the deuterated data in the bulk embryont cluster set, so both sets were combined and fit linearly in $n^{-1/3}$ giving equation (21) where σ_G is in eV with an estimated standard deviation of 0.013 eV. Again, the smooth progression of the absorption data to a known bulk value means that the photoelectron data must also progress smoothly (without transitions) to a meaningful bulk value. The bulk Gaussian widths of the e^-(aq) bulk absorption spectra show a similar indifference to deuteration [$\sigma_G = 0.3041(15)$ eV for non-deuterated *vs.* $\sigma_G = 0.3010(8)$ eV for fully deuterated]. As will be more fully discussed in section 6.3, this suggests that the range of thermal solvent fluctuations accessible in the excess electron's ground state is the same upon deuteration. Consequently, observed differences in the breadth of the low-energy side of the photoelectron *vs.* absorption spectra are likely due to differences in the slopes of the upper electronic state potential curves in an ion solvation coordinate that are accessed in these processes, i.e. whether the conduction band or excited p-state is accessed.

The Lorentzian widths: Unlike the E_{max} and σ_G parameters, the Lorentzian widths (σ_L, characterizing the high-energy side of the spectra and the dynamics at work) of both the absorption and photoelectron $(H_2O)_n^-$ cluster data sets were extensively overlapped (see bottom of Figure 1). The fits have already been described in section 4.1. The $(H_2O)_n^-$ photoelectron and absorption spectra have very similar blue tails, for instance at $n = 50$, the fitted values of σ_L are 0.48 ± 0.06 and 0.46 ± 0.06 eV, respectively. This suggests a common dynamical limitation. In the case of the non-deuterated combined set, it appears that the Lorentzian widths reach a bulk value at $n \sim 60$, i.e. well before bulk. On the other hand, σ_L is affected by deuteration. A fit of the $(D_2O)_n^-$ photoelectron data gave equation (22) where σ_L is in eV with an esd of 0.03 eV. The fitted deuterated results are smaller than the non-deuterated clusters by 0.07 eV at $n = 11$ and 0.05 eV at $n = \infty$, which is consistent with the bulk difference at 210 K of 0.044 eV. The deuterated data reaches the bulk value at $n \sim 71$ (as compared to $n \sim 60$, 67, or 55 for the non-deuterated). Clearly, there is a component of nuclear motion regarding the blue asymmetric tail of the lineshape. When these σ_L observations are coupled to the vibrational peak observations,[8] it suggests that electronic–vibrational mixing should be investigated.

$$E_{max,\,PES,\,H_2O}(n) = VDE_n = -5.65(16)n^{-1/3} + 3.25(6) \tag{19}$$

$$E_{max,\,PES,\,H_2O/D_2O}(n) = VDE_n = -5.38(15)n^{-1/3} + 3.15(6) \tag{20}$$

$$\sigma_{G,\,PES,\,H_2O/D_2O}(n) = -1.02(5)n^{-1/3} + 0.548(19) \tag{21}$$

$$\sigma_{L,\,ABS/PES,\,H_2O}(n) = -1.61(18)n^{-1/3} + 0.90(7) \quad \text{for } n \leq 60 \tag{18}$$

$$\sigma_{L,\,PES,\,D_2O}(n) = -1.66(28)n^{-1/3} + 0.85(11) \quad \text{for } n \leq 71. \tag{22}$$

5. Main result: extrapolating the photoelectron lineshape to bulk

Much of the photoelectron spectrum of the bulk hydrated electron is immediately evident from the fitted cluster values of E_{max} and σ_G when $n = \infty$. The bulk photoelectron lineshape parameters are $E_{max} = 3.25(6)$ eV and $\sigma_G = 0.548(19)$ eV corresponding to a nominal temperature of 210 K. Since the value of σ_L reaches bulk at a finite size ($n = \sim 60$), it is not definitively determined. We assume that $\sigma_L = 0.493$ eV which is the same as the bulk absorption value by virtue of the similarity of photoelectron and absorption spectral trends. However better data (less scatter over a larger cluster size range) might give a different result. The photoelectron and absorption normalized spectral lineshapes of the bulk hydrated electron at 210 K are given in Figure 2 for comparison. They are considerably different (and the explicit bulk photoelectron value of σ_L has little effect on the comparison since it is a high-energy tail and absorption is at lower energy). These differences are particularly important if the photoelectron spectrum is a good approximation to the photoemission spectrum.

6. Other results and discussion

The following experimental observations make a convincing case for the meaningful extrapolation of the bulk embryont cluster group data to bulk: (1) the bulk $n^{-1/3}$ slope of the cluster photoelectron peak centre (VDE) data, (2) the lack of any observed cluster groups having larger VDEs than the bulk embryonts,[38] (3) the smooth $n^{-1/3}$ progression of the peak centres and Gaussian widths of cluster absorption lineshapes as well as properties derived from the lineshape (radius of gyration and average kinetic energy of the excess electron) to known bulk values, and (4) the enhancement of the lower binding energy states upon deuteration indicating that the transformations or inter-conversions from dipole bound to intermediate to bulk embryonts are ones of increasing electron internalization. The surface/internal debate is very important regarding the interpretation of our extrapolated results, so in the two following sections we examine the issue in more detail.

6.1. *Additional experimental evidence for internalization of the excess electron*

By operating at very high source pressures Neumark and coworkers[12] observed long-sought surface states in large water cluster anions in addition to the ones we observed at smaller sizes.[8] This work came 'fast on the heels' of two time-resolved photoelectron studies on water cluster anions, one by Zewail and coworkers[13] and the other by Neumark and coworkers.[26] Based on the lifetime trends of excited p-states, both groups concluded that internalized excess electron states were likely to exist in the water cluster anions they had studied. Recent infrared multiple photon dissociation spectra[39] show that the excess electron interacts with multiple water molecules above $n = 25$ as would be expected with internalization. The Neumark group photoelectron studies show colder source conditions favouring $(D_2O)_n^-$ surface states[12] over the bulk embryont group and they suggested a kinetic barrier at low temperatures to the solvent reorientation associated with electron internalization. Consequently, it can be surmised that the warmer conditions (lower source backing pressures) of our experimental ion source would be more likely to allow the solvent reorganization associated with internalization.

6.1.1. *Evidence based on photoelectron spectral intensity upon deuteration*

In our warmer experiments, all three groups of species are in evidence in the size range of $n = 11$–16, so this is a critical region where such species are likely to have comparable free energies. At any given cluster size, the lower electron binding energy species (dipole bound and intermediate groups) are always observed to gain in spectral intensity relative to the bulk embryonts upon deuteration[8] as illustrated for $n = 11$ in Figure 3.

A simplified model was created to consider the effect of deuteration on the relative stabilities of comparable-energy cluster structures (of the same number of water molecules) with hydrogen bonding networks of different strengths. In Figure 4 hydrogen bonding is

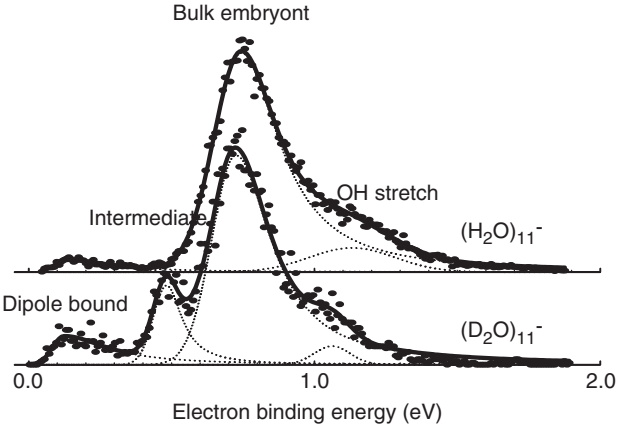

Figure 3. Photoelectron spectra of $(H_2O)_{11}^-$ and $(D_2O)_{11}^-$ showing multiple isomers. The lower binding energy isomers are more abundant upon deuteration.

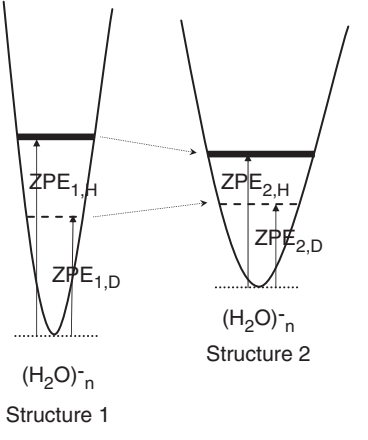

Figure 4. Simple schematic of the hyperdimensional potential energy surfaces of two different structures of similar energy for a cluster anion with n waters. Structure 1 (on left with a less-internalized excess electron and stronger H-bonding) is pictured changing into Structure 2 (on right with a more-internalized excess electron and weaker hydrogen bonding). The non-deuterated energy levels are indicated with solid lines while the change upon full deuteration is indicated with a dotted line. This schematic depicts how deuteration is more stabilizing to the structure with stronger H-bonding.

represented by wells in a hydrogen bonding coordinate. A narrow well corresponds to stronger hydrogen-bonding with larger force constants, whereas a wide well corresponds to weaker hydrogen bonding with smaller force constants. The zero point energies of the non-deuterated structures are shown with heavy solid lines of similar energy. Noting that the process of making a cavity for an electron in water is one of reducing the hydrogen bonding between nearby water molecules, the curve for the well on the left (Structure 1) of Figure 4 is narrow as would be expected for weaker interactions of the excess electron with the water cluster, i.e. interactions that are less disruptive of the hydrogen bonding network. The curve on the right (Structure 2) of Figure 4 is wider as would be expected for stronger interactions of the excess electron with the water cluster, i.e. interactions that are more disruptive of the hydrogen bonding network. The narrower well can be expected to have a greater change in energy upon deuteration (as illustrated with dotted lines in Figure 4), so structures corresponding to weaker electron–water cluster interactions can be expected to experience greater stabilization upon deuteration.

Here we quantify this effect under the assumption of quasi equilibrium for a transformation of an *n*-water cluster of a less-internalized excess electron species (Structure 1) into a more-internalized species (Structure 2) as shown in Figure 4. The numbers are, of course, only as good as the assumptions, and the results should be taken as rough estimates. The difference in the equilibrium concentrations of non-deuterated species Structure 1 and 2 (denoted [1,H] and [2,H] and the same equilibrium with deuterated species (denoted [1,D] and [2,D] gives

$$-RT\ln\frac{[2,H]}{[1,H]}+RT\ln\frac{[2,D]}{[1,D]}=\left(ZPE_{1,D}-ZPE_{1,H}\right)-\left(ZPE_{2,D}-ZPE_{2,H}\right)+\left(\Delta G_{1,D}^{0\to T}-\Delta G_{2,D}^{0\to T}\right)+\left(\Delta G_{2,H}^{0\to T}-\Delta G_{1,H}^{0\to T}\right) \quad (23)$$

where $\Delta G^{0\to T}$ is the free energy change upon taking the system from 0 K to a finite temperature T for each species, ZPE is the total zero point energy of all vibrations in the cluster, and the ratios of concentrations are taken from the relative observed abundances (from the last column of Table 1 in of our preceding paper).[8] Since both species Structure 1 and 2 have the same number of water molecules, the free energies of thermalization are nearly cancelling giving the following approximation

$$-RT\ln\frac{[2,H]}{[1,H]}+RT\ln\frac{[2,D]}{[1,D]}\approx\left(ZPE_{1,D}-ZPE_{1,H}\right)-\left(ZPE_{2,D}-ZPE_{2,H}\right) \quad (24)$$

where R is the gas constant, and T is taken as 210 K (based on considerations from section 4.1). The differences in the difference of ZPE upon deuteration [right-hand side of Equation (24)] are given in Table 2 for the three possible transitions between the dipole bound, intermediate, and bulk embryont groups. Considering a transition from Structure 1 (with a weaker excess electron–cluster interaction) to Structure 2 (with a stronger excess electron–cluster interaction), the difference in the differences of ZPE upon deuteration should be negative, i.e. the Δ(ZPE) for Structure 2 should be less than the Δ(ZPE) of Structure 1, where these are defined as $ZPE_{2,D}-ZPE_{2,H}$ and $ZPE_{1,D}-ZPE_{1,H}$, respectively. Notably at $n=12$, we have all three species represented in both the deuterated and non-deuterated spectra. The difference in the difference of ZPE upon deuteration for the dipole-bound→bulk embryont transformation at $n=12$ is –0.064 eV or –520 cm^{-1} which is

Table 2. Difference in the difference of zero point energy (ZPE) [right side of equation (24)] pertaining to equilibria between the dipole bound-like, intermediate, or bulk embryont states upon deuteration as determined by observed relative intensities [see equations (23) and (24)] under the assumption of a 'quasi' equilibrium in the cluster ion source and a temperature of 210 K.

n	Dipole-bound → Bulk embryont (eV)	Intermediate → Bulk embryont (eV)	Dipole bound → Intermediate (eV)
6			−0.023
7			−0.014
11	−0.020		
12	−0.064	−0.024	−0.040
13		−0.032	
14		−0.046	
16		−0.028	

large compared to kT at 210 K (146 cm^{-1}). Most importantly, all entries in Table 2 are negative showing that all of the reactions as written in Table 2 are more internalizing with regard to the excess electron. This quantitatively confirms the simpler qualitative expectations developed with Figure 4 and the preceding paragraph. The Table 2 results provide structural evidence that the electron is internalizing as we go from the dipole bound, to intermediate, to bulk embryont states, i.e. evidence that the hydrogen bonding is increasingly disrupted as the excess electron becomes more stabilized in the cluster. The bulk embryont group is observed as the last group on the road to internalization.

6.2. *Discussion of theoretical results on internalization of the excess electron*

Ab initio and density functional (multi-electron) calculations of clusters in the size range of our bulk embryonts are beginning to appear in the literature. They have daunting difficulties associated with a large numbers of atoms, diffuse electron states, vast numbers of possible H-bonded isomers,[40–43] and finite temperature effects.[12,44] K.S. Kim and coworkers performed[45] searches for promising structures of $(H_2O)_{12}^-$ and investigated four of the more stable ones with various degrees of excess electron internalization at the MP2/6-311++G**//HF//6-31++G* level. The 'partially internal' structure had good agreement with the bulk embryont experimental vertical detachment energy. Kahn[46] has identified an internal cavity structure for $(H_2O)_{14}^-$ at the MP2/6-311+G*//MP2/aug-cc-pVDZ level and has studied surface and internal structures[47–49] with B3LYP methods for $(H_2O)_n^-$ where $n = 20$, 21, and 24. Herbert and Head-Gordon[55] have more systematically examined the reliability of MP2 and B3LYP calculations for calculating VDEs of $(H_2O)_n^-$ systems up to $n = 24$. In general, internal, surface, and intermediate states have been identified by theory in this size regime, but definitive conclusions regarding the surface/internal nature of the experimental bulk embryonts will require more work. Based on CCSD(T) *ab initio* work, Wang and Jordan[50] have developed a quantum Drude oscillator model for the excess electron that enables the modelling of electron correlation effects. Applying this work to larger cluster anions, Jordan and Sommerfeld[44,51] find that favourable electrostatics including second-order dispersion effects are not sufficient to bind an excess electron in a favourable cavity. Higher-order electron correlation effects are needed for binding within a

cavity and to obtain the larger VDEs associated with systems like the experimental bulk embryont group. It is likely that a very good treatment of electron correlation will be required to decide between surface and internal states. It also seems that one-electron models that do not include high-orders of electron correlation could easily underestimate the stability of internalized cavity systems. As computer power increases, more multi-electron, *ab initio* based pictures are emerging of the excess electron and the fluxional nature of its cavity.[24,52] While a cavity picture may be a good zero-order description, there is always some excess electron density lying outside the cavity which no doubt facilitates some of the non-cavity-like behaviours[53] of the hydrated electron.

Pioneering simulations of Landman and coworkers (QUPID),[9–11] as well as recent simulations by Turi *et al.*,[14] predict the existence of both surface and internal states of hydrated electron clusters, and indeed there is experimental evidence for both. Both of these simulation methods treat only one electron quantum mechanically. The capabilities and limitations of one-electron models for hydrated electrons have been addressed in a review by Shkrob.[54] Multi-electron *ab initio* methods[44,55] and Jordan and Sommerfeld's[44,51] analysis (favourable electrostatics are not enough to stabilize a cavity electron) show that extensive electron configuration is required to get the energetics correct, so there is a need for energetic verification and calibration of one-electron models. Landman's calculated surface states coincided with the experimental bulk embryont VDEs and, on the that basis, they interpreted our original experimental data as being indicative of surface states, but the $n^{-1/3}$ slope of their calculated internal state VDEs (–9.8 eV) is almost twice the continuum value based on the static and optical dielectric constants of water. The calculated intercepts are also unrealistically large. Turi *et al.*[14] interpret the experimental data as surface states, even though the experimental bulk embryont VDEs fall midway between their calculated values for internal and surface states. Some of the conclusions of Turi *et al.* were immediately challenged.[12] In this regard, note that Turi *et al.*'s calculated internal states[14] at 100 K (see Figure 3B therein) show a $n^{-1/3}$ slope of ~12 eV (more than a factor of two beyond the dielectric limit), i.e. they are not calibrated regarding the connection to bulk. Their model yields internal state clusters with ground state radii of gyration, $\sqrt{\langle r^2 \rangle} = 2.2$ Å, a bit smaller than the bulk experimental value of 2.43 Å based on Equation (12a) and kinetic energy, $\langle KE \rangle = 1.95$ eV, which is larger than the bulk experimental value of 1.58 eV by Equation (13a). More curiously, s-p transition energies, $\sqrt{\langle r^2 \rangle}$, and $\langle KE \rangle$ of the theoretical internal states do not change with cluster size. This model suggests that there is little difference between the internal cavity formed by the smallest cluster and that at bulk. This is a theoretically testable idea and it would be useful to see what multi-electron theory predicts on this issue. Landman's electron–water pseudopotential was also less than ideal[34] because clusters at $n = 32$, 64, and 128 had interior states with radii of gyration of ~2.1 Å at 300 K (tighter than the experimental bulk value of 2.43 Å based on Equation (12a)). The moment analysis results of Equation (12a) [or (12b)] show that the radius of gyration is largest in the smallest cluster and that it gets smaller towards bulk, not the other way around. The same QUPID calculations also have $\langle KE \rangle$ of ~2.4 eV for the cluster anions [~0.8 eV higher than the bulk value of 1.58 eV by Equation (13a)]. The moment analysis results of Equation (13a) [or (13b)] show that $\langle KE \rangle$ is small in the smallest cluster and that it gets bigger towards bulk. It is clear that with a radii too tight and kinetic energy too high, the QUPID method will overestimate E_{max} and in particular VDEs. These problems are likely correlated with calculated $n^{-1/3}$ trends of

VDEs exceeding the dielectric limit by a factor of two. In our opinion, calibrated calculations would give lower calculated VDEs for both the surface and internal states. In fact Verlet *et al.*[12] have pointed out that scaling of the QUPID results by 60% gives very satisfactory agreement with the surface and internal VDEs of both the Bowen and Neumark[12] groups. A smaller scaling of the Turi *et al.* results by ~75% also gives satisfactory agreement with experiment.

The bulk embryonts are the cluster group progressing smoothly to the inherently internalized bulk hydrated electron, so why not call them the internal state group? After all, they correlate to the bulk internal state. Nevertheless, being in a group that is more internalized than the dipole bound and intermediate states, and being a group that is internalizing does not mean that internalization is complete in any of the clusters, particularly the smallest in the series. The process of internalization with increased cluster size is likely to be gradual, as implied by Equation (14), i.e. it does not involve a surface to internal transition at a specific cluster size. Entropy may be decisive in the gradual internalization process as proposed[37] for $I^-(H_2O)_n$. Considering the large size of dipole bound electrons, it is probably significant that at $n = 11$, the 3.5 Å radius of gyration of the excess electron [Equation (14)] is only a bit smaller than the 4.3 Å radius of a globular cluster of 11 water molecules. This system will exhibit much surface character, even though it is well along the road to internalization compared to dipole bound systems and even if the centre of the excess electron distribution is internal. So we choose the name bulk embryonts, rather than internal or surface states, because gradually internalizing systems will have some characteristics of both. The name bulk embryonts emphasizes that their properties connect smoothly to bulk, without regard to the degree of internalization at $n = 11$.

6.3. *Interpretation of spectral results in terms of excited state potential curves*

If an electron is bound in a sufficiently shallow spherical well, it may support only one bound state (ground s-state) and no bound excited states. The first excited state (p-state) is said to be virtual and embedded in the conduction band (continuum). In this case, Kajiwara *et al.*[56] have shown how to calculate the absorption spectrum from the photoemission spectrum giving a blue asymmetric tailing of the absorption spectrum that can be modeled to fit experiment. There is a long history of such models[57,58] variously called polaron or bound–free models. At $n = 11$, as can be seen in Figure 5, the photoelectron (closed circles) and absorption spectra[35] (open symbols) are very similar in position, shape, and width. Since the experimental absorption data lacks its low-energy side, half of this assertion can be credited to the fits of section 4.1 (solid line is the fitted absorption lineshape). The similarity demonstrates that photon-scanned absorption and photoemission, and photon-fixed photoelectron spectra all have the same lineshape at this size (usually they are different). Therefore all transitions in the absorption spectrum at this cluster size produce the same upper states as does photoemission (necessarily free electron states). A shallow well provides no bound excited states and the absorption is fully modeled by photodetachment.[56]

However, as n increases, the electron well grows deeper and p-states come into play. *p*-states have been demonstrated both at bulk[19–21,23–25] and in clusters.[13,22,26] Johnson and coworkers[22] first observed the excited p-state growing in smoothly with cluster size [as a

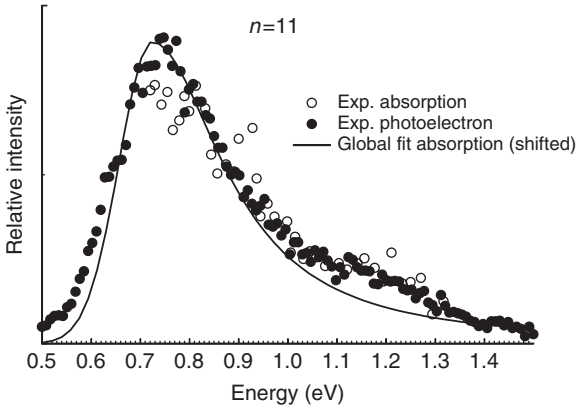

Figure 5. The experimental photoelectron (closed circles) and absorption spectra (Ref. 35, open circles) at $n = 11$ have been overlayed to show their similarity. The global fit, absorption lineshape (offset by 0.09 eV due to the difference in a global fit of parameters vs. a lineshape fit of an individual spectrum) is also shown to help fill-in the missing low-energy portion of the experimental absorption lineshape. The similarity of the photoelectron and absorption lineshapes at $n = 11$ argues that bound excited states are not important upon photoexcitation of clusters this size.

second, two-photon peak of lower binding than normal using ultrafast resonant two-photon photodetachment of $(H_2O)_n^-$] and both the Zewail[13] and Neumark groups[26] have seen cluster p-state dynamics approaching bulk dynamic values with increased cluster size. Any entirely bound-to-free model[56,58] cannot accommodate a difference in the absorption and photoemission spectra. Given the similarity of the photon-fixed photoelectron and photon-scanned photoemission lineshapes, the separation of the absorption and photoelectron spectra is attributed to the development of p-states which stabilize with increased clustering. The photoelectron/photoemission spectra access the conduction band, while the absorption spectra access both the conduction band and p-states in general, but primarily the p-state at bulk.

The spectral differences of the absorption and implied photoelectron spectra are quite pronounced at bulk (see Figure 2 or the right side of Figure 6). There is a fair sized gap between the maxima of these spectra, and the gap is large compared to any possible temperature effects. These effects can be understood in the context of vertical photo-access (see Figure 6) from the ground state of e^-(aq) to excited state potential energy curves (p-state or conduction band) as weighted by the probability of having a particular ground state configuration (indicated with a dashed curve labeled 'distribution' on the left side). Note that the ground state potential curve has a minimum at some configuration of water molecules about the excess electron charge. The conduction band rises in the anionic solvation coordinate,[59] (see Figure 6 therein) because there is no localized charge to stabilize solvating molecule arrangements. The p-state (less localized than the ground state, but more localized than the conduction band) is intermediate and has a minimum at lower values of the anionic solvation coordinate. Since the region accessed in both upper states is far from the adiabatic minima of these curves,[29] the spectroscopy corresponds to a projection of the ground state solvent configurations onto repulsive portions of the upper state curves.

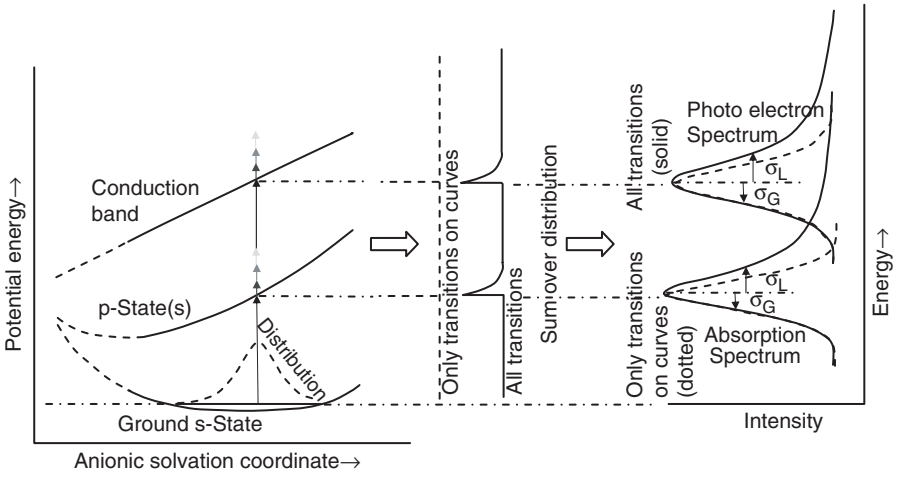

Figure 6. A potential energy diagram of the hydrated electron in an anionic solvation coordinate (left). In this coordinate, only repulsive portions of the upper states (p-states and conduction band) are accessible from the ground state. The darkest arrows represent transitions from the most probable, ground state, solvation structure to the upper state potential curves in the static approximation. Additional transitions are shown on the potential diagram (right) that fall above the upper state curves. They become less intense as they get further from the potential curve (as indicated by fading from black). The traces in the middle of the figure show the spectral contributions of the most probable solvation structure in the static approximation (dashed) and with all transitions (solid). After summing all spectral contributions weighted by the ground state distribution (dotted curve at left), one obtains the spectra (at right) in the static approximation (dashed) and for all of the transitions (solid). Lorentzian spectral tails result when a power law models the diminishing access away from upper state potential curves.

The significant difference in the peak centres (E_{max}) of the bulk absorption versus photoelectron spectra attest to absorption access to a lower curve (i.e. p-states) than the conduction band. This idea is reinforced by significant differences in the Gaussian widths (σ_G). The absorption σ_G is 0.259 eV (Jou/Freeman) or 0.304 eV (Tuttle/Golden) and compares to a value almost twice as big, 0.548 eV, in the photoelectron spectrum. The Gaussian widths demonstrate a smaller slope for the electronic potential curve of the p-states (accessed in absorption) as compared to the conduction band (accessed in the photoemission or photoelectron spectra) in the anionic solvation coordinate at the hydrated electron ground state. The excited p-states are not embedded in the conduction band at the region of vertical access at bulk.

The Lorentzian profiles of spectral lineshapes, as characterized by σ_L, are particularly interesting. The parameter, σ_L, is a half-width-at-half-maximum (HWHM) and is always greater than the Gaussian HWHM (1.177 σ_G). Dynamics are associated with the Lorentzian tails preventing the observation of the static-approximation prediction of full Gaussian lineshapes (dashed spectral curves on the right side of Figure 6). There have been great computational difficulties[19,60–66] in obtaining the *singular* Lorentzian tail of the experimental bulk absorption spectrum suggesting to us that the explanation is not in the models. The absorption spectrum shows its Lorentzian tail long before there is significant access to the conduction band at the peak of the photoelectron spectrum, so the

conduction band is not the direct source of the Lorentzian tail in the absorption spectrum. Instead, the absorption and photoelectron lineshapes share a similar σ_L width at any particular cluster size revealing a similar dynamics independent of whether the p-states or conduction band are accessed. The sensitivity of σ_L to deuteration and the disappearance of vibrational features with increasing cluster size suggest a nuclear component in the electronic excitation process. As either upper state is accessed, the system promptly changes to one with optimal structures of less strong solvation. Initial ultrafast solvent motions (reorientations and intramolecular vibrational motions) are likely to be similar independently of which upper level is accessed, since the finals states in each case are less charge-localized than the initial state. We suggest that a coupling of nuclear motion and electronic degrees of freedom is required to get the observed Lorentzian tails. This is illustrated on the left side of Figure 6 with transitions (vertical black arrows) directed to the upper state potential curves (the static approximation) and additional transitions accessing the region just above the upper state potential curves (these give rise to the blue spectral tails). Each transition just above the potential curve can be associated horizontally along the solvation coordinate with an isoenergetic transition on the potential curve – one allowed in the static approximation. As transitions get further above the potential curve, they are weaker (indicated by lighter arrows) because they have further to go along the anionic solvation coordinate to get to their corresponding, isoenergetic, static-approximation-allowed transition on the potential curve. The middle of Figure 6 shows the contribution of the most likely ground state configuration to the spectra when only transitions to the potential curve are considered (dashed trace, static approximation) and when a power law governs diminishing access away from the curve (solid trace). If traces like these are summed over and weighted by the ground state distribution of configurations, one obtains the absorption and photoelectron spectra shown on the right side of Figure 6. The dashed traces show the static approximation result, while the solid traces are sketches of the experimental results. The transitions of diminishing access above the electronic curves may be related to solvent fluctuations (along the anion solvation coordinate) and/or charge hopping that have been described in certain theoretical descriptions.[52,67,68]

6.4. *Experimental bulk photoelectron threshold and the condensed phase electron affinity of ice, V_0*

Thresholds, partially obscured by thermal initial population and exponentially decaying density of final trapping states, are still extractable with empirical threshold laws as long as one has photo-access to the states at the band edge. In water, we usually do not have access to such states because water molecules dramatically reorganize themselves about a charge.[69] A photoionization product requires a significant difference in the arrangement of waters, so vertical photo-processes run out of solvent overlap between the initial and final states at the band edge. Such behaviour produces exponential spectral tails without thresholds. The quantity V_0 (also called the condensed phase electron affinity) is the energy required to promote a delocalized, conducting electron of minimal energy into vacuum with zero kinetic energy. It is a measure of the energy from the vacuum level to the bottom

of the conduction band. In the absence of solvent overlap effects, V_0 can be determined by subtracting the photoemission threshold from the photoconductivity threshold. In the presence of solvent overlap effects, one must examine the whole lineshape in the threshold spectral region. In Figure 2, we have plotted Kevan's[70] observed photoconductivity spectrum of hydrated electrons in ice (open symbols) along with the bulk photoelectron spectrum obtained from extrapolating the cluster data (solid line). Considering that Kevan's data was recorded at 77 K, while the cluster data is thought to pertain to a nominal temperature of 210 K, we have added an offset of −0.32 eV as determined by Equation (2a) to the Kevan data to bring it to 210 K. After this temperature adjustment, we find that the photoconductivity threshold region falls almost exactly on top of the photoelectron threshold region. This reinforces the observed similarities between photon-fixed photoelectron and photon-scanned photoemission spectra and suggests that $V_0 \approx 0.0$ eV in ice.

A good discussion of V_0 in water has been given by Han and Bartels.[71] Jortner's considerations[65] found that $-0.5 < V_0 < 1.0$. Henglein,[72,73] who performed calculations on systems where solvent reorganization was important, found a value of –0.2 eV. Apparently V_0 is much smaller in magnitude than past experimental values, such as the value of -1.2 ± 0.1 eV given by Grand, Bernas, and Amouyal.[74] Their value may need reinterpretation due to the use of non-polar solvation models and in consideration of recent observations on the change in the conduction band and vacuum level energies with the ion solvation coordinate.[59,75] A number of arguments have been presented previously,[59,75] in favour of a small V_0 value in water. Given that water and ice have similar dielectric properties, the value of V_0 in water may not be significantly different than in ice.

6.5. VDE_∞, the radius of gyration, and extrapolating a gradual internalization trend

The parameter $n^{-1/3}$ derives from the reciprocal of cluster radius, and as presently used ignores the excess electron's contribution to the cluster's volume. This issue can potentially change the intercept of the peak centres upon extrapolation to bulk, and the matter is further complicated by the fact that the excess electron's volume changes as a function of cluster size. The radius of gyration of Equation (14), that was determined with moment analysis, shows the gradual internalization of the excess electron as the cluster size increases. Using the radius of gyration *vs.* n of Equation (14), we determined $\beta(n)$, the volume of the excess electron in units of the volume of a bulk water molecule, as

$$\beta(n) = \frac{(4/3)\pi[R(n)]^3}{31.73} \tag{25}$$

where $R(n)$ is the radius of gyration in Å, 31.73 Å^3 is the volume of a water molecule at 210 K, such that β is unitless. By these criteria and at 210 K, the volume of the excess electron is equivalent to 5.62 water molecules at $n = 11$, falling to 2.78 water molecules at $n = 69$, and to 1.53 water molecules at bulk. The $(H_2O)_n^-$ cluster VDEs have been plotted against both $n^{-1/3}$ and $(n+\beta)^{-1/3}$ in Figure 7. The use of $(n+\beta)^{-1/3}$ seems to produce more curving of the data at the smallest cluster sizes, particularly at $n = 10$–13. In order to allow for gradual curvature [i.e. a situation where the excess charge might gradually, with

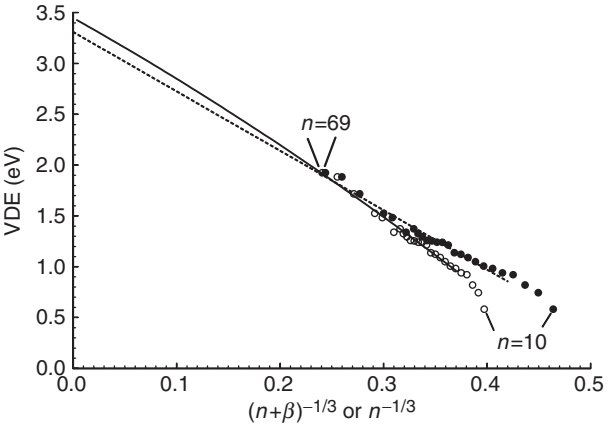

Figure 7. Given the possibility that the excess charge only gradually and entropically samples the centre of the bulk embryont clusters with increasing cluster size, $(H_2O)_n^-$ photoelectron VDEs are plotted *vs.* both $n^{-1/3}$ (filled circles, dotted line) and $(n+\beta)^{-1/3}$ (open circles, solid line) where n is the number of waters and β is the volume of the excess electron in units of the volume of a bulk water molecule. The latter abscissa allows the excess electron to be included in the cluster's total volume.

increasing cluster size, sample more of the cluster's centre – in a manner similar to that proposed[37] for $I^-(H_2O)_n$], we fit the data against $(n+\beta)^{-1/3}$ leaving out $n=10$–13 and fixing the limiting slope to the continuum value (−5.702 eV at 210K), to find

$$\mathrm{VDE}(n) = 3.449(33) - 5.702(n+b)^{-1/3} - 2.76(30)(n+b)^{-2/3} \tag{26}$$

where VDE is in eV. This procedure produces $\mathrm{VDE}_\infty = 3.45 \pm 0.03$ eV which compares favourably with $\mathrm{VDE}_\infty = 3.25 \pm 0.06$ eV from the $n^{-1/3}$ fit of Equation (19). We report our value of VDE_∞ as 3.4 ± 0.2 eV to account for these systematic errors of extrapolation, in particular gradual internalization. This quantity is a unique determination with no known bulk counterpart. The most probable reorganization energy for arranging water molecules about the electron is 1.7 eV as determined by subtracting the electron's hydration enthalpy from VDE_∞.

7. Conclusion

The parameters that govern the whole lineshape of $(H_2O)_n^-$ photoelectron spectra have been extrapolated to bulk yielding the implied photoelectron spectrum of the bulk hydrated electron. There is much more information in the whole lineshape of $(H_2O)_n^-$ photoelectron spectra than that obtained from our preliminary work on peak centres. The unexpected similarities in the lineshapes of the absorption and photoelectron spectra has led to the conclusion that the fixed-wavelength photoelectron spectra are very similar to wavelength-scanned photoemission spectra due to projection of ground state configurations onto repulsive portions of the upper state potential curves as viewed in an anionic solvation coordinate. Important conclusions result from the comparison of absorption and photoelectron lineshapes, particularly at bulk. To facilitate this comparison, we established an average temperature of the cluster data and a set of

temperature-consistent relations for the absorption lineshape parameters and properties extractable from the lineshape (radius of gyration and average kinetic energy) through moment analysis. Among other things, these properties allow us to characterize the size of the gradually internalizing excess electron and to account for its effect on the bulk extrapolated value of the vertical detachment energy. The photoelectron and absorption spectra are very similar in shape, width, and position at $n = 11$, and different (yet retaining some similarities) at bulk, showing the development of bound excited states of the excess electron with cluster size. The bulk hydrated electron's absorption spectrum exhibits Lorentzian tailing in a region where the photoelectron spectrum reveals little access to the conduction band. Therefore the tailing is not due to an embedded or virtual p-state, but rather to a common initial response of the solvating water molecules whether the hydrated electron is promoted to the p-state or the conduction band. The 'question of whether the electron is broadly delocalized' has been asked since early spectral observations of solvated electrons.[76] A dynamic answer to this question arises from the σ_L width parameters. The clusters achieve bulk dynamic behaviour in σ_L at finite cluster sizes ($n = 60$ with non-deuterated and $n = 71$ with full deuteration) providing a measure of the range of the excess electron's dynamical effect on the solvent. Finally, the bulk photoelectron spectrum was compared to photoconductivity data reinforcing the similarity with photoemission lineshapes and showing that V_0 (the condensed phase liquid electron affinity) is about zero in ice.

Acknowledgements

This material is based in part upon work supported by the National Science Foundation under Grant No. CHE-0517337 (KB). This material is also based in part upon work supported by the National Science Foundation under Grant No. CHE-0413077 (JC). JC also thanks the ACS PRF (42452-AC5) for support. Both JC and KB thank T.R. Tuttle and D.M. Bartels for valuable discussions.

References

[1]J.V. Coe, Ph.D. Dissertation, The John Hopkins University (1986).
[2]S.T. Arnold, J.V. Coe, J.G. Eaton, C.B. Freidhoff, L. Kidder, G.H. Lee, M.R. Manaa, K.M. McHugh, D. Patel-Misra, H.W. Sarkas, J.T. Snodgrass and K.H. Bowen, 'Photodetachment Spectroscopy of Negative Cluster Ions', The Chemical Physics of Atomic and Molecular Clusters, G. Scoles, Amsterdam, Elsevier, 467 (1990).
[3]J.V. Coe, G.H. Lee, *et al.*, J. Chem. Phys. **92** 3980 (1990).
[4]G.H. Lee, S.T. Arnold, J.G. Eaton, H.W. Sarkas, K.H. Bowen, C. Ludewigt and H. Haberland, Z Phys. D: At. Mol. Clusters **20**(1–4) 8 (1991).
[5]H. Haberland and K.H. Bowen, 'Solvated electron clusters', Springer Ser. Chem. Phys. **56**(Clusters of Atoms and Molecules II) 134 (1994).
[6]A.W. Castleman and K.H. Bowen, Jr., J. Phys. Chem. **100**(31) 12911 (1996).
[7]J.V. Coe, A.D. Earhart, *et al.*, J. Chem. Phys. **107** 6023 (1997).
[8]J.V. Coe, S.T. Arnold, *et al.*, J. Chem. Phys. **125** 14315 (2006).
[9]R.N. Barnett, U. Landman, *et al.*, Phys. Rev. Lett. **59** (7), 811 (1987).
[10]R.N. Barnett, U. Landman, *et al.*, J. Chem. Phys. **88**, 4429 (1988).
[11]R.N. Barnett, U. Landman, *et al.*, J. Chem. Phys. **88** (7), 4421 (1988).

[12]J.R.R. Verlet, A.E. Bragg, *et al*., Science **310** (5755), 1769 (2005).
[13]D.H. Paik, I.R. Lee, *et al*., Science **306** (5696), 672 (2004).
[14]L. Turi, W.S. Sheu, *et al*., Science **309**, 914 (2005).
[15]F.-Y. Jou and G.R. Freeman, Can. J. Chem. **57** (5), 591 (1979).
[16]T.R. Tuttle and S. Golden, J. Chem. Soc., Faraday Trans. **2** (77), 873 (1981).
[17]J. Kim, I. Becker, *et al*., Chem. Phys. Lett. **297** (1–2), 90 (1998).
[18]T.R. Tuttle Jr, S. Golden, *et al*., Radiation Phys. Chem. **32** (3), 525 (1988).
[19]J. Schnitker, K. Motakabbir, *et al*., Phys. Rev. Lett. **60** (5), 456 (1988).
[20]A. Wallqvist, G. Martyna, *et al*., J. Phys. Chem. **92** (7), 1721 (1988).
[21]D.H. Son, P. Kambhampati, *et al*., J. Phys. Chem. A **105** (36), 8269 (2001).
[22]J.M. Weber, J. Kim, *et al*., Chem. Phys. Lett. **339** (5–6), 337 (2001).
[23]P. Kambhampati, D.H. Son, *et al*., J. Phys. Chem. A **106** (10), 2374 (2002).
[24]M. Boero, M. Parrinello, *et al*., Phys. Rev. Lett. **90** (22), 226403/1 (2003).
[25]C. Nicolas, A. Boutin, *et al*., J. Chem. Phys. **118** (21), 9689 (2003).
[26]A.E. Bragg, J.R.R. Verlet, *et al*., Science **306** (5696), 669 (2004).
[27]D.M. Bartels, K. Takahashi, *et al*., J. Phys. Chem. A **109** (7), 1299 (2005).
[28]S. Golden and T.R. Tuttle Jr, J. Phys. Chem. **82** (8), 944 (1978).
[29]S. Golden and T.R. Tuttle Jr, J. Chem. Soc., Faraday Trans. 2 **75** (3), 474 (1979).
[30]S. Golden and T.R. Tuttle, J. Chem. Soc., Faraday Trans. **2** (77), 889 (1981).
[31]S. Golden and T.R. Tuttle, J. Chem. Soc., Faraday Trans. **2** (77), 1421 (1981).
[32]I. Carmichael, J. Phys. Chem. **84** (10), 1076 (1980).
[33]D.J. Lavrich, P.J. Campagnola, *et al*., NATO ASI Ser., Ser. B **326** (Linking the Gaseous and Condensed Phases of Matter: The Behavior of Slow Electrons), 183 (1994).
[34]D.M. Bartels, J. Chem. Phys. **115** (9), 4404 (2001).
[35]P. Ayotte and M.A. Johnson, J. Chem. Phys. **106** (2), 811 (1997).
[36]P. Ayotte, G.H. Weddle, *et al*., J. Chem. Phys. **110** (13), 6268 (1999).
[37]J.V. Coe, J. Phys. Chem. A **101** (11), 2055 (1997).
[38]A. Kammrath, J.R.R. Verlet, *et al*., J. Chem. Phys. **125** (7), 076101/1 (2006).
[39]K.R. Asmis, G. Santambrogio, *et al*., J. Chem. Phys. **126** (19), 191105/1 (2007).
[40]M.D. Tissandier, S. J. Singer, *et al*., J. Phys. Chem. A **104** (4), 752 (2000).
[41]J.-L. Kuo, J.V. Coe, *et al*., J. Chem. Phys. **114** (6), 2527 (2001).
[42]J.-L. Kuo, C.V. Ciobanu, *et al*., J. Chem. Phys. **118** (8), 3583 (2003).
[43]J.-L. Kuo and S.J. Singer, Phys. Rev. E: Statistical, Nonlinear, and Soft Matter Physics **67** (1–2), 016114/1 (2003).
[44]T. Sommerfeld and K.D. Jordan, J. Am. Chem. Soc. **128** (17), 5828 (2006).
[45]J. Kim, J.M. Park, *et al*., J. Chem. Phys. **106** (24), 10207 (1997).
[46]A. Khan, J. Chem. Phys. **125** (2), 024307/1 (2006).
[47]A. Khan, J. Chem. Phys. **118** (4), 1684 (2003).
[48]A. Khan, J. Chem. Phys. **121** (1), 280 (2004).
[49]A. Khan, Chem. Phys. Lett. **401** (1-3), 85 (2005).
[50]F. Wang and K.D. Jordan, J. Chem. Phys. **116** (16), 6973 (2002).
[51]T. Sommerfeld and K.D. Jordan, J. Phys. Chem. A **109** (50), 11531 (2005).
[52]I. Park, K. Cho, *et al*., Computational Materials Science **21** (3), 291 (2001).
[53]G.W. Robinson and H.F. Hameka, Proc. SPIE-Int. Soc. Opt. Eng. **742**, (Laser Appl. Chem. Dyn.) 82 (1987).
[54]I.A. Shkrob, The structure and dynamics of solvated electron in polar liquids. Los Alamos National Laboratory, Preprint Archive, Physics: 1-45, arXiv:physics/0701071 (2007).
[55]J.M. Herbert and M. Head-Gordon, Phys. Chem. Chem. Phys. **8** (1), 68 (2006).
[56]T. Kajiwara, K. Funabashi, *et al*., Phys. Rev. A **6** (2), 808 (1972).
[57]D.A. Copeland, N.R. Kestner, *et al*., J. Chem. Phys. **53** (3), 1189 (1970).

[58]V.D. Lakhno and N.L. Leonova, Izvestiya Akademii Nauk Seriya Fizicheskaya **64** (8), 1458 (2000).
[59]J.V. Coe, A.D. Earhart, *et al.*, J. Phys. Chem. **107**, 6023 (1997).
[60]J. Schnitker, P.J. Rossky, *et al.*, J. Chem. Phys. **85** (5), 2986 (1986).
[61]J. Schnitker and P.J. Rossky, J. Chem. Phys. **86** (6), 3462 (1987).
[62]J. Schnitker and P.J. Rossky, J. Chem. Phys. **86** (6), 3471 (1987).
[63]P.J. Rossky and J. Schnitker, J. Phys. Chem. **92** (15), 4277 (1988).
[64]M. Sprik, J. Phys. – Condensed Matter **2**, SA161 (1990).
[65]F.J. Webster, J. Schnitker, *et al.*, Phys. Rev. Lett. **66** (24), 3172 (1991).
[66]B.J. Schwartz and P.J. Rossky, J. Chem. Phys. **105** (16), 6997 (1996).
[67]A. Banerijee and J. Simons, J. Chem. Phys. **68** (2), 415 (1978).
[68]B. Webster, J. Phys. Chem. **84** (10), 1070 (1980).
[69]J. Jortner, Ber. Bunsenges. Phys. Chem. **75** (7), 696 (1971).
[70]L. Kevan, J. Phys. Chem. **76** (25), 3830 (1972).
[71]P. Han and D.M. Bartels, J. Phys. Chem. **94** (15), 5824 (1990).
[72]A. Henglein, Ber. Bunsenges. Phys. Chem. **78**, 1078 (1975).
[73]A. Henglein, Can. J. Chem. **55**, 2112 (1977).
[74]D. Grand, A. Bernas, *et al.*, Chem. Phys. **44**, 73 (1979).
[75]J.V. Coe, Int. Rev. Phys. Chem. **20** (1), 33 (2001).
[76]L.M. Dorfman, F.Y. Jou, *et al.*, Berichte der Bunsen-Gesellschaft **75** (7), 681 (1971).
[77]F.-Y. Jou and G.R. Freeman, J. Phys. Chem. **83** (18), 2383 (1979).